Journal of Thermal Biology 79 (2019) 56–68

Contents lists available at ScienceDirect

Journal of Thermal Biology

journal homepage: www.elsevier.com/locate/jtherbio

Thermal effects of mobile phones on human auricle region

Joanna Bauer[a,*], Charlie O'Mahony[b], Drahomir Chovan[b], John Mulcahy[b], Christophe Silien[b], Syed A.M. Tofail[b]

[a] Faculty of Fundamental Problems of Technology, Department of Bioengineering, Wroclaw University of Science and Technology, Wybrzeze Wyspianskiego 27, Wroclaw 50-370, Poland

[b] Department of Physics, and Bernal Institute, University of Limerick, National Technological Park, Limerick, Ireland

ARTICLE INFO

Keywords:
Biological heat transfer
Thermal model
Mobile phone
Health impact of mobile phone
IR thermography
Personalized and preventive medicine

ABSTRACT

Mobile phones have become an indispensable utility to modern society, with international use increasing dramatically each year. The GSM signal operates at 900 MHz, 1800 MHz and 2250 MHz, may potentially cause harm to human tissue. Yet there is no *in silico* model to aid design these devices to protect from causing potential thermal effect. Here we present a model of sources of heating in a mobile phone device with experimental verification during the phone call. We have developed this mobile phone thermal model using first principles on COMSOL® Multiphysics modelling platform to simulate heating effect in human auricle region due to mobile phone use. In particular, our model considered both radiative and non-radiative heating from components such as the lithium ion battery, CPU circuitry and the antenna. The model showed the distribution and effect of the heating effect due to mobile phone use and considered impact of battery discharge rate, battery capacity, battery cathode material, biological tissue distance, antenna radio-wave frequency and intensity. Furthermore, the lithium ion battery heating was validated during experiments using temperature sensors with an excellent agreement between simulated and experimental data (< 1% variation). Mobile phone heating during a typical call has also been simulated and compared with experimental infrared thermographic imaging. Importantly, we found that 1800 MHz frequency of data transmission showed the highest temperature increase in the fat/water phantom used in this simulation. We also successfully compared heating distribution in human auricle region during mobile phone use with clinical thermographic images with reasonable qualitative and quantitative agreements. In summary, our model provides a foundation to conceive thermal and other physical effects caused by mobile phone use and allow for the understanding of potential negative health effects thus supporting and promoting personalized and preventive medicine using thermography.

1. Introduction

With more than 4.57 billion users around the world since 2017 (Statista.com, 2016), mobile phone is now an indispensable feature of modern life. Every day in the UK alone, 20% of males and 24% females make at least one call using their mobile phones (Statista.com, 2018). Mobile phones use radiofrequency (RF) waves for communication. It falls within the larger electromagnetic radiation spectrum and raises concerns regarding potential health hazards of thermal effects especially the body parts that are in direct contact with mobile phone during use.

International Agency for Research on Cancer (IARC) has classified mobile phone radiation as "possibly carcinogenic to humans" (group 2B on the IARC scale) (IARC, 2013). Due to the potential harm, exposure to electromagnetic waves is regulated. In the European Union (EU), the European Committee for Electrotechnical Standardization (CENELEC) specify the maximum allowed localized specific absorbance rate (SAR) to be less than 2 W/kg averaged over the 10 g of tissue (Council of European Union, 1999) for the head region. In the United States, Federal Communications Commission (FCC) guidelines put the maximum permissible exposure level to the public at 580 μW/cm^2 (F.C.Commission, 2015), which is in with the guidelines of National Council on Radiation Protection (NCRP). According to the FCC maximum exposure from mobile phones must be less than SAR level of 1.6 W per kilogram (1.6 W/kg) averaged over 1 g of tissue (F.C.Commission, 2015). Currently, there is no model that could help designing mobile phones so that its thermal effect can be quantitatively controlled thus reducing its overall health impact during use.

In large doses, radio frequency waves in the electromagnetic spectrum can break down tissues and damage deoxyribonucleic acid (DNA).

* Corresponding author.
E-mail address: joanna.bauer@pwr.edu.pl (J. Bauer).

https://doi.org/10.1016/j.jtherbio.2018.11.008
Received 3 October 2018; Accepted 12 November 2018
Available online 14 November 2018
0306-4565/

Though, due to the relatively low levels of exposure of mobile devices, its level of harm from long-term exposure to humans is still unknown and direct correlations to brain tumours have not been established (Kundi, 2004; WHO.int, 2016). The consensus is though, to minimize exposure time. The health impact of radiofrequency communication due to mobile phone use in the literature is mostly derived from animal and human studies. Some of these studies indicate a positive correlation between the exposure to radiofrequency (3 kHz to 300 GHz) on living organisms including human and a higher risk of developing pathology malignant brain tumours such as glioma, meningioma, acoustic neuroma or astrocytoma (IARC, 2013; Durney et al., 1986; Hepworth et al., 2006; Khurana et al., 2009). There are also studies that conclude with opposite results (Prasad et al., 2017; Dreyer et al., 1999; Schüz et al., 2006; Deltour et al., 2012).

Literature, however, generally agrees on the adverse effect of mobile phone use on the users' cognitive and comfort response (Little et al., 2012; Kim et al., 2016; Koivisto et al., 2000a,b; Krause et al., 2004), potential neuropsychiatric disorders (Krause et al., 2000), sleep pattern disruptions (Abdel-Rassoul et al., 2007; Borbely et al., 1999; Huber et al., 2002), attention deficiency, increased fatigue, irritability, anger or anxiety (Mann and Röschke, 1996; Oftedal et al., 2000) and sensations (Krause et al., 2000), phantom vibrations and ringing syndrome (Acharya et al., 2013), male fertility (Goyal, 2015) and reproductive processes (Agarwal et al., 2008). It is also mostly agreed that children are a far bigger risk group. In fact, children including fetuses are more susceptible to electromagnetic radiations due to higher tissue conductivity and thinner skull bone (Hamada et al., 2011; Morgan et al., 2014).

Computer models of radiative heating and heat transfer to the user can provide objective, physiological insights by providing physical routes and quantity of heat and radiation transfer from mobile phones to body during use. As potential health hazard of mobile phone use is most likely to be due to cumulative exposure leading to chronic impact, such models can also provide a proper platform of long-term impact of mobile phone usage under several usage scenarios that are not possible to articulate in animal or human subjects. It can help to determine potential health impact *in silico* prior to carrying out any in vivo animal or human investigation in accordance to the 3R principles (Replacement, Reduction and Refinement) of ethical use of animals and ensuring safety to human subjects.

Mobile phone use affects human tissues both non-thermally and thermally. Interactions with magnetic and electrical fields are non-thermal effects of which the former is more influential in penetrating human body (Christ et al., 2010) than the latter. Anatomical structure, chemical composition and electrical properties such as the electric permittivity and conductivity of tissues or organs cause the response to electromagnetic field to vary (Carl et al., 1986). For example, skin, bone, blood, muscles, epithelial or neural tissues differently absorb radiofrequency (Cleveland et al., 1997; Habash, 2008). Electromagnetic radiation (including microwaves) can change plasma membrane structure and functionality (Robertson et al., 2006; Neumann et al., 1982), cause DNA damage (Lai and Singh, 1996; Blank and Goodman, 1999), activate/deactivate cell enzymes (De Iuliis et al., 2009; Panagopoulos, 2011; Simon et al., 2000), alter conformations of proteins (Kesari et al., 2011), and calcium-potassium ions efflux (Laurence et al., 2000; Ha, 2001). Heating and mechanical strain can also make protein and amino acid crystals to generate electrical charge, physiological significance of which is still unknown.

Thermal effect is one of the principal factors affecting physiological processes in human body. Microwave-generated thermal effect include heat conduction to other tissues, convection through blood perfusion and radiation to the surrounding tissues (Blackman et al., 1982). Thermal effects on living objects aren't always uniform. For example, skin surface temperature distribution is influenced by the intensity of heat stimulus, stimulus duration as well as the external environment of stimulation influences the thermal distribution (Adair et al., 1984). Heat can be accumulated by tissues due to disturbed organism's homeostasis caused by disproportion between the heat generation and dispersion. Such accumulation can give rise to chronic effects, as there can be disruption of cell functions and development due to thermal effects (Kundi, 2004). In the case of mobile phones, current literature considers risks of thermal impact as more detrimental than that from the dipole polarization of biomolecules and tissues.

From an exposure point of view, human auricle region is the most potent anatomical part during mobile phone use for both thermal and non-thermal effects. Efforts in the direct measurement of thermal changes to mobile phone users during the use of mobile phones include:

a. The use of negative temperature coefficient (NTC) thermistors (Tahvanainen et al., 2007)
b. Infrared (IR) thermography for quantitative analysis of local heating in ears at two different specific absorption rate (SAR) (Kargel, 2005)
c. IR thermography to measure thermal change in both contact and non-contact use of mobile phones (Lahiri et al., 2015) and
d. IR thermography to isolate quantitatively the respective effects of radiative and battery heating of the anatomical part in contact that can accumulate to a pathological development over the years (Bauer et al., 2018).

The so called 'smartphones' generally have much lower SAR and much higher battery capacity when compared to the older mobile phones. This means that while radiative heating can be minimized through filtering, battery heating can be significant but generally unaccounted for. There are models that investigates thermal effects in, e.g. lithium (Li) ion batteries using Multiphysics modelling platforms such as COMSOL® (Lai et al., 2015; Hosseinzadeh et al., 2017; Cai and White, 2011). The impact of smart mobile phone use, especially respective contributions of radiative and non-radiative heating and non-thermal effects in the zone of use, is not known. This leads us to use human head model for simulating thermal impact of mobile phone so that mobile phone SAR can be related to the potential risk to sensitive organs and tissue in the human body.

Developing an accurate human head model requires the incorporation of thermal and electromagnetic properties of tissues and organs in head into the simulation. Each of these properties undergo changes with respect to temperature. For example, relative permittivity can decrease by ~0.12% for every single (°C) change in temperature (De Iuliis et al., 2009). The geometry and the shape of the head model as well as thickness and size of its various components such as skin, cartilage, skull, brain will also be important to consider. This means that a head model must be constructed taking in to account properties that non-uniformly vary (Simon et al., 2000). Previous RF and SAR models (Li et al., 2014; Develi and Sorgucu, 2015) studied the radiation effect of variation of tilt angles and distance of the phone from the head (Iqbal-Faruque et al., 2014). However, thermal affects from battery and other sources in the phone must also be counted for.

The Joule heating contributes heat to Li-ion battery through conduction thus affecting its discharge and heat energy released. On the other hand, RF heating originates from the absorption of electromagnetic waves and does not contribute to heat conduction. Due to this, frequency dependence of dielectric properties of various components of Li-ion batteries, must be considered while developing a model. The relative resonance frequency and dielectric constant of the mobile phone antenna also changes with temperature, which, in turn, affects its output frequency (Sanders et al., 2015; Mernyei and Volgyi, 1990), and must be considered.

Here, we simulate a combination of radiative and non-radiative heating of auricle region of human head using first principles within a finite element Multiphysics simulation platform COMSOL®. We built a model of mobile phone battery taking into consideration of its materials, geometry and performance parameters such as discharge, capacity, cathode material and the state of electrical charge. We then

experimentally tested thermal effects during battery heating in real life to compare with that in the COMSOL® model as the battery fully discharges.

Unlike previous models in the literature, our model combine thermal effects from RF heating with thermal impact from the mobile phone that originate from the battery and other components such as f-shaped integrated antenna and central processing unit (CPU). In this way, our model brings about a design aspect by incorporating all potential thermal sources and sinks in a mobile phone. We provide the outputs of the simulations in heat maps so that non-contact IR thermography can be used for using these models in designing clinical studies as well as analysing clinical data.

2. Materials and methods

In our model we take into account of both radiative (RF) and non-radiative (battery, CPU and antenna) heating in mobile phones and translate into human head model. The model incorporates changeable parameters that influence the thermal management of a mobile phone. This allows us to monitor heat transfer from mobile phone to the nearby regions of head that is in direct contact with phone, somewhat mimicking previous clinical study. Simulations produced output in thermographic form to provide meaningful interpretation relevant to *in vivo* thermographic data.

We also include a short experimental investigation on battery heating during discharging. Temperature, voltage and current in these experimental tests were recorded using PASCO® data loggers. The electrical circuit experiment will involve placing probes for temperature, current and voltage around the phone and its battery, then utilizing the results in fine-tuning of the model. Fig. 1 shows the experimental set up and circuit diagram. A temperature sensor was placed directly on the batteries surface and measuring the current (A) and voltage (V) over a known resistance. The experiment was kept as thermally insulated with the use of a Styrofoam box around the circuit, preventing convection cooling. The experiment also involved placing the phone within a box and visualizing the thermal energy using a thermal camera under different phone call conditions e.g. a 3 min call.

The modelling involved a numerical description of heating to be implemented using finite element method in COMSOL® Multiphysics simulation platform (COMSOL Multiphysics®), which seamlessly connects the head model with the mobile phone model. Simulations combined COMSOL modules on lithium ion battery, electrical heating, radiofrequency and biological heat transfer. The detailed methodology of the model building and simulations are described below.

2.1. Lithium ion battery heating model

A more precise simulation of thermal effects from a battery will need quantitative information of its configuration, physical geometry, and chemical and electrical properties to be included in the model. This may be impractical from a computational resource point of view and a simplification is necessary to provide necessary information within a reasonable time. For this, we assumed a layered structure in the battery that would allow very little variation in the local phenomena within the layers, and neglect heat transfer at the boundaries between layers. The layered structure thus makes the battery a pseudo-homogenous material that can be represented in two dimensions for heating. Such a 2D model (Krause et al., 2004) can still simulate the thermal phenomenon of the Li-ion Battery (LIB) with reasonable accuracy (Kim et al., 2016) but with much faster speed and less resources.

For designing the lithium ion batteries thermal properties, the chemical reaction can be simplified as a 2D line. This line acts as a linear version of the battery, with only one dimension of ion movement. Generally, during operation of a Li-ion battery, the heat-generation follows the equation (Chen et al., 2005)

$$\mathrm{Q} = \frac{\mathrm{I}}{\mathrm{Vol}}\left(\mathrm{U} - \mathrm{V} - \mathrm{T}\frac{\partial \mathrm{U}}{\partial \mathrm{T}}\right) \tag{1}$$

where Q is the total heat, I the total current of the battery, Vol the total volume, U the open circuit potential, T the temperature and V the working voltage. Eq. (1) however does not fully account for the thermal effects of the electrochemical model. Lithium ion battery generates heat from by electrochemical reactions (Q_{reac}) active, reversible polarization (Q_{rev}), and ohmic losses (Q_{ohm}), which are described as follows (IARC et al., 2013):

$$Q_{reac} = FaJ(\phi_1 - \phi_2 - U) \tag{2}$$

$$Q_{rev} = FaJT\frac{\partial U}{\partial T} \tag{3}$$

and

$$Q_{ohm} = \sigma_{eff}\left(\frac{\partial \phi_1}{\partial x}\right)^2 + \kappa_{eff}\left(\frac{\partial \phi_2}{\partial x}\right)^2 + \frac{2\kappa_{effRT}}{F}(1-t_+^0)\frac{\partial (lnc)}{\partial x}\frac{\partial \phi_2}{\partial x} - \phi_2 - U \tag{4}$$

where F is the Faradays constant of electrochemical reaction, a the specific interfacial area, J the pore wall flux of lithium ions, ϕ_1 the electrochemical potential in the solid phase, ϕ_2 the electrochemical potential in the electrolyte, T the absolute temperature, σ_{eff} the effective electrical conductivity, κ_{eff} the effective electrochemical reaction rate constant, R the resistance, t_+ the transference number of lithium ion, and c the concentration of the electrolyte (Cai and White, 2011).

The total energy balance can then be found from

$$\rho C_p \frac{dT}{dt} = \lambda \frac{\partial^2 T}{\partial x^2} + Q_{reac} + Q_{rev} + Q_{ohm} \tag{5}$$

where ρ is the density of the electrolyte, C_p the heat capacity at constant pressure, T is the temperature and t the time.

The 2D model described in Eq. (5) in terms of temperature change over time is comparable to thermography which measures changes in temperature. The model accounts for the porous electrode theory assuming that the electrolyte/pores are homogenously distributed and

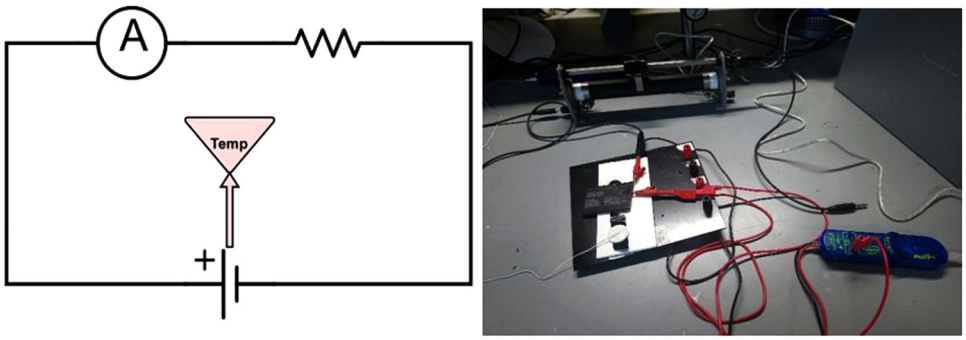

Fig. 1. Circuit diagram and experimental set up for measuring battery heating for a 200 s call.

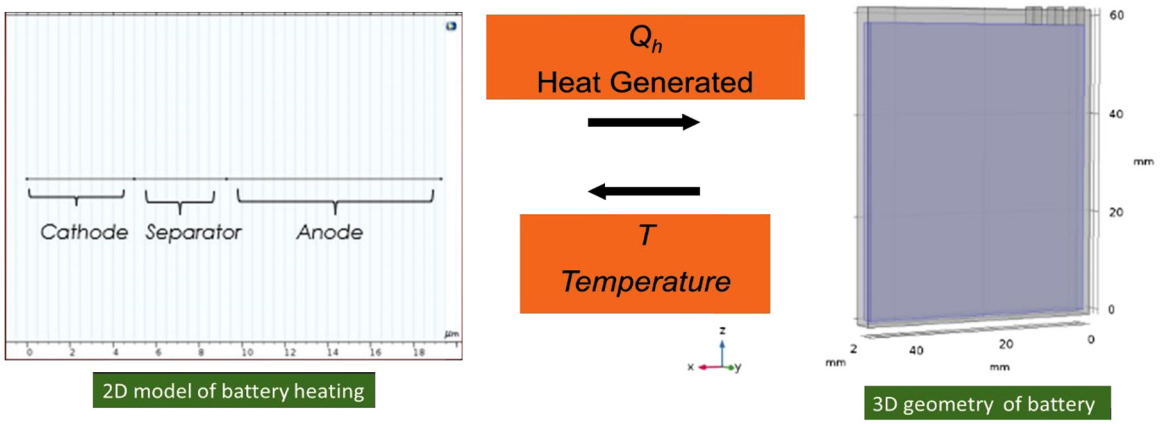

Fig. 2. Two-dimensional reduction of thermal effect for Li-ion battery used in 3D geometry of lithium ion battery in COMSOL®. The shaded area represents the thermally active portion of the battery within the geometric modelling within mutually orthogonal axes x-y-z.

composed of spherical particles. The Bruggeman volume averaging method accounts for effective electrochemical transport properties (Tjaden et al., 2016). Using D and ε to denote the respective transport coefficients and volume fractions of the two separate media A and B, for which $\varepsilon_A \ll \varepsilon_B$, the effective transport coefficient is given by (Tjaden et al., 2016):

$$\frac{D_{eff} - D_B}{D_{eff} + nD_B} = \Lambda \frac{D_A - D_B}{D_A + D_B} \tag{6}$$

where $\Lambda = \varepsilon_A/\varepsilon_B$, with n = 2 for spheres (as in this simulation)

The 2D model also accounts for the Ohms law, mass transfers, solution concentrations and kinetics of the intercalation of lithium ions. As all relevant factors contribute to an average heat generation, a coupling of this 2D model into a 3D geometry can be taken as an acceptable methodology for heat transfer due to electrode discharging/charging. Due to the temperature dependence of heat, the 3D geometric model must be fed back into the 2D thermal model (Fig. 2). The parameters used for simulation using this model are given in Table 1.

2.2. Circuit board heating simulation

Joule heating, otherwise known as Ohmic heating is the process where electrical energy passing through a resistor is converted into heat. Joule's first law states that the power of the heating generated by electrical conduction is proportional to the product of its resistance and the square of the current, $P \propto I^2R$.

Table 1
Parameters used in developing the thermal model of Li-ion battery in COMSOL.

Parameter	Value	Unit
Battery		
Lengths: cathode, separator, anode	5, 4.3, 10	mm
Material: cathode, separator, anode, electrolyte	Lithium Cobalt Oxide, Polyethylene, Graphite, LiPF6 in 3:7 EC: EMC	–
Salt Concentration	1200	Mol/m^3
State of Charge	100	%
Battery Cell Capacity	1.4	Ah
Discharge rate	0.8, 0.6 and 0.4	mA
Dimensions	50 × 60 × 3 (w/ casing)	mm
Antenna		
Frequency	1800	MHz
Antenna terminal voltage	10	V
Antenna shape	f-shape	–
Impedance	~50	Ω
Heat transfer		
Initial temperature	23.2	°C

For simulating heating in the circuit board, the circuitry is considered as an averaged, single resistor for Joule heating while ignoring the fact that during use the resistance of the phone's CPU can vary. This generalization for Joule heating is acceptable as we are primarily looking at phone call use rather than CPU use for data reception and use for example in the use of mobile apps. CPU's do not continuously heat, however as they throttle their input power to maintain a nominal operational temperature. We incorporated a step function into the heating calculation that allows the heating value to decrease as it reaches the maximum run- temperature (Fig. 3).

2.3. Simulation of RF heating

Mobile phone communication uses RF waves absorbed in and radiated by the phone antenna, which can create a considerable amount of thermal energy during RF reception and transmission. Mobile phone thermal models therefore need to take in to account RF heating (dielectric heating) of the antenna. Dielectric heating occurs due to the molecular rotation of a dipoles in a material when excited by electromagnetic waves due to the tendency of dipoles to align along the direction of the electromagnetic field (Koivisto et al., 2000a,b). If the field is oscillating, as it is in an electromagnetic wave, these molecules rotate continuously in tandem generating thermal energy loss. The common frequencies used for dielectric heating ranges from 3 MHz to 30 GHz, which includes the RF communication frequency range of 900–1800 MHz).

The power, P absorbed by radio frequency waves in a dielectric, is given by:

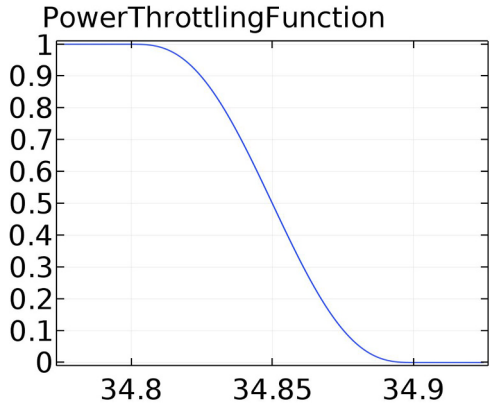

Fig. 3. Step function used to simulate CPU heating, y axis being the ratio of power used, 1 being nominal and 0 being none. X axis is the temperature, 308 K.

$$P = 2\pi f \varepsilon_0 \varepsilon'' E^2 Vol \quad (7)$$

where f is the frequency of the RF, ε_0 permittivity of the free space, ε'' the imaginary part of complex dielectric constant, E the electric field strength and Vol the material volume. A crucial factor contributing to the potential hazard associated with dielectric heating is the depth to which the electromagnetic waves penetrate, which is governed by the Beer-Lambert law, which establishes that the intensity of an electromagnetic wave transmitted from the surface into the material decays exponentially:

$$I(z) = I_0 e^{-\alpha z} \quad (8)$$

where, I_o, α and z denote the initial intensity, the linear attenuation and the depth of penetration respectively.

The penetration depth, PD in human tissues by incident rf waves is given by (Komarov et al., 2005):

$$PD = \frac{2}{\alpha} = \frac{\lambda_{rf}}{2\pi} = \sqrt{\frac{2}{[\sqrt{(\varepsilon_r')^2 + (\varepsilon_r'')^2}) - \varepsilon_r']}} \quad (9)$$

where λ_{rf}, ε', ε'' denote the RF wavelength and the real and imaginary part of complex dielectric constant respectively.

The RF module in COMSOL® has been used to calculate the heating and penetration depth of the radiowaves produced by a phone antenna. Eq. (5) outlines the general heating power generated for these simulations.

2.4. Estimation of SAR

The energy being absorbed from radiofrequency fields, by biological systems, is frequency dependent. Health risks associated with exposures to radiofrequency heating are directly linked to absorption and distribution of the energy in the body. Specific absorption rate (SAR) is a measure of the rate at which energy is absorbed by the human body when exposed to a radio frequency electromagnetic field, measured in Watts per kilogram (Chen and Steckner, 2017). SAR, the main component of which, in the current case, is microwave radiation to and from the mobile phone, quantifies this. In testing phone antennae for SAR, the phone is placed against a human head phantom specially designed to respond similarly to biological compositions in head and a call is simulated in the region of mobile phone use. The highest value point of absorption in the entire head is taken as the SAR value. From a medical point of view, RF absorption should be minimized as much as possible. Acceptable limits of SAR have been set on mobile devices.

The SAR of the simulation is given by (Iqbal-Faruque et al., 2014):

$$E_{SAR} = \sigma \frac{|E|^2}{\rho} \quad (10)$$

where σ, E and ρ is the electrical conductivity, electrical norm and density respectively.

Work into mobile phone Specific Absorption Rate has been modelled and tested in various papers (Iqbal-Faruque et al., 2014; Develi and Sorgucu, 2015; COMSOL Muliphysics®, 2011). Though, linking this with a mobile phone battery model a total overarching simulation for mobile phone thermal effects can be determined. These results will present a more comparable model with clinical test trials for mobile phone use, as in Bauer et al. (2018).

3. Results and discussion

3.1. Joule heating of mobile phone battery

The setup shown in Fig. 4 was used to measure the surface temperature of battery using resistor loads of 5 Ω, 7.5 Ω, and 10 Ω. The same set up was used to measure the surface temperature of the screen of the mobile phones during a 200 s phone call. This experiment shows the combination of all thermal effects, as the antenna, battery and

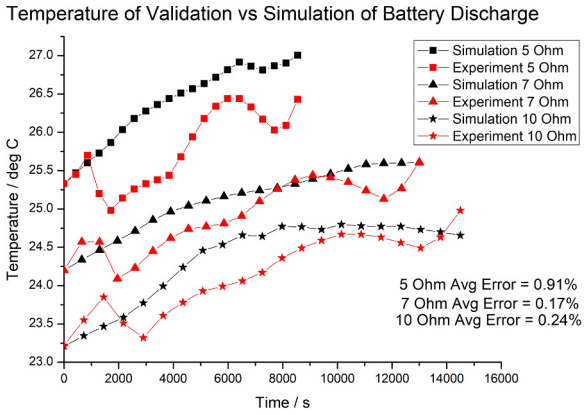

Fig. 4. A comparison of simulation and experimental Joule heating of mobile phone batteries.

circuitboard are active. This gives the phone surface temperature data. All network connections will be disabled before and after the call, using "flight mode". Flight (aeroplane) mode is an inbuilt setting to deactivate all network connections, this will ensure that the temperature change is from the antenna alone. With parameter variation the model can inform us on the influence into a mobile phones thermal energy. Firstly, comparing the simulation of the lithium ion battery with the validation testing. By taking the ambient parameters and variables in the experimental validation test and inputting them into the battery model, the accuracy of the lithium ion battery model can be determined. The surface temperature of the lithium ion battery in both experiments is what will be investigated, at the centre of the body of each battery.

Fig. 4 shows a comparison between the Joule heating of batteries simulated using the methodology described in Section 2 and experimental. While the overall trends were emulated, the experiment and simulation vary in detail especially in the time cycles of oscillation in temperature increase. While, simulation showed a gradual, steady increase of temperature over time, experiments showed some dips and rise in the temperature increase. This may be due to some heat-throttling mechanisms built in the battery by its manufacturer to protect from overheating during use. Despite such mechanisms, experimental tests showed an increase in temperature of between 1 and 1.5 °C over the 15,000 s (4 h and 10 min).

To simulate the ohmic resistance as a discharge (as voltage and current vary with discharge) the current discharge was set by Ohms law, where the voltage of the battery is fed back into the discharge rate, divided by the set resistance. The variation in the 5 Ω measurements could notably be from not fully allowing for the battery to relax to ambient temperature, this initial value is used in the simulation, as even 0.2 °C less on the simulation would show a high level of agreeance. It is important to note also that on the temperature curves for the experimental, an initial drop is seen, this likely accounting for the endothermic reaction of the cathodes. Initially at low discharge rates, the chemical reactions enthalpy energies dominate the overall heat production of the battery.

For the voltage curve (Fig. 5b), the validation experimental voltage drops much quicker to a nominal voltage, ~3.7 V then the simulation, which holds a nominal voltage of ~4.0 V. Since the current is proportional to this voltage, similar results are seen in the current curve. A potential cause of this variation is ageing of the phone battery, as lithium ion batteries degrade in efficiency with successive charge/discharge cycles. As the simulation is an idealized lithium ion battery of this design, depreciation of the materials or any other non- idealized factor effects the open circuit voltage of the anode and cathode.

The validation experiment measured from the centre of the battery in operation, whereas these values in the simulation are the average

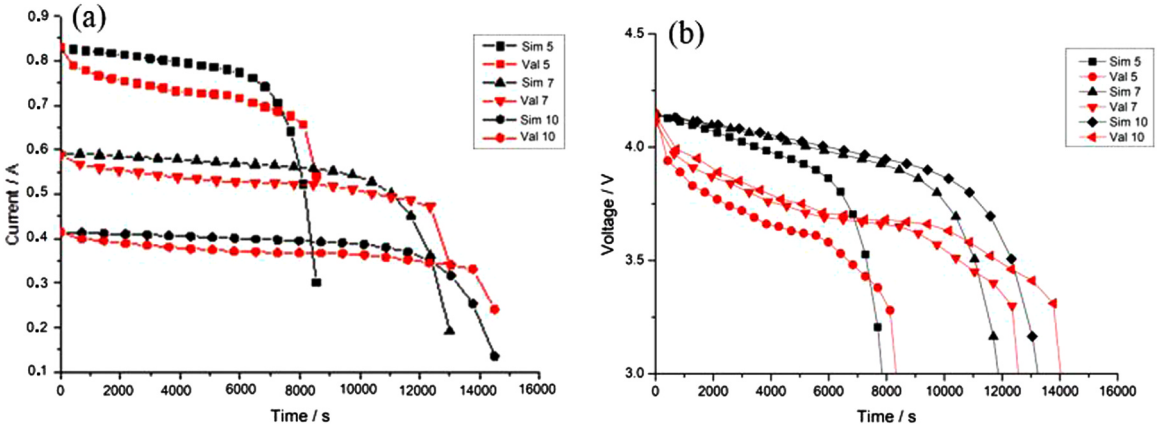

Fig. 5. Simulated and experimental current vs time plot during Joule heating of an idealized LCO battery showing overall resemblance of the behaviour (a). This is not true for voltage vs time plot (b).

temperature across the lithium ion component. For a closer similarity to the validation experiment, measurement of the 2D surface temperature of the battery in each simulation, would present a closer similarity. Setting up each discharge rate at the same initial temperatures. In this instance, the casing of the phone battery plays more of a significant role. To cover this mix of possible polyethylene terephthalate layers, polymer layers, and polypropylene layers, an average polymer material was used. These 2D surface in Fig. 6 images shows comparable results to the validation, at the centre of the 2D surface. Variations arise from precise material, geometry details and ageing of battery. For a more accurate battery model in any continuation study, X-ray Computed Tomography could be conducted for internal geometries, including foils and casings (NTS News Center, 2016).

Fig. 6 shows the comparison of mean temperature at the centre of a lithium ion battery at 0, 30 and 60 min of 8A discharge between 2D COMSOL simulated images and experimental infrared imaging under the same discharge and initial conditions. The mean temperature of the battery surface in both the simulated and experimental images show excellent agreement an acceptable error from the validation, as the variation in each from the experimental value was less than 1%. This provides an excellent basis for going forward with our model further simulations as described in the next sections. Looking at the impacts of various battery parameters, the simulation results show to us that a) battery temperature increases with discharge rate, b) cathode materials show the highest temperature increase with Lithium Cobalt Oxide (LCO), the most commonly used commercial material, whereas Lithium Manganese Oxide (LMO) showed a temperature decrease c) temperature decreases with increase in battery capacity.

3.2. Effect of circuit board heating

Amalgamating the circuit board to the nominal discharge of the battery, the resulting temperature for the complete non-radiative thermal effects of the phone is found. Due to smartphones having input temperature monitors for the CPU and battery, an active comparison can be made with this model. This was found to be 30–35 °C varying load on the CPU and 26–29 °C for the battery. Comparing this to the simulated combination of battery and CPU, a 2D surface and slice is taken of the simulation. This is shown in Fig. 7. The circuit board and battery combination proved effective, showing comparable results, in simulating the temperature across the phone thus allowing experimental testing of phone temperatures. For the variation of antenna power and frequency, power directly increases RF heating and is discussed in the following section.

3.3. Antenna: frequency variation

Mobile phones operate at three different frequency bands, 900 MHz, 1800 MHz and 2350 MHz. Setting up the simulation for the antenna to output at each frequency, a comparison of the frequencies impact can be made. At the voltage input used, temperature increases in the phantom from 1 h of exposure are shown in Fig. 8. Temperature distribution shown in the top graphs and the log of the norm of the electric field along the bottom, mapping the intensity changes of the norm of the electromagnetic field. Fig. 8a and d show that at 900 MHz frequency, the maximum temperature in the antenna increases by a nominal 0.06 °C in the air surrounding the phone, 0.05 °C in about 40 mm into the sample. The penetration of heat runs all the way through the sample. Electromagnetic field is absorbed by the fat phantom but disperses out in the y-direction, which is in the opposite side of the fat with respect to the phone. Electromagnetic intensity shows a conduction of radiation through the fat as the field intensity is notably high on out the back of the phantom.

Much more pronounced heating is seen at 1800 MHz, with heating of 1 °C seen at 90 mm deep into the sample (Fig. 8b). The maximum temperature increase (2 °C) is seen in the fat phantom. The electromagnetic field intensity is also larger, almost by a factor of 1.5 to that seen at 900 MHz. The intensity at this frequency is mainly seen in the air (Fig. 8e). The frequency of 2250 MHz shows a maximum temperature change of 0.07 °C but with a similar temperature distribution and intensity range as that seen at 1800 MHz (Fig. 8f). For each of the frequencies investigated, we see the largest intensity of the electromagnetic field to occur in the air gap between the phone and the phantom. The 1800 MHz showed the highest field intensity, with 2250 MHz having similar field strengths.

3.4. Antenna: variation of call duration

Fig. 9 shows a graph of simulated and experimentally observed temperature from temperature sensor mimicking a 200-s phone call. The first 12 s allowed the measurement of the ambient temperature of screen (25 °C), after which the network connection was turned on to initiate the 200-s phone call. The network connection was then turned off using “aero plane mode”. Convective cooling was then allowed for further 370 s.

The model shows good agreement between the experimental temperatures of the phone screen with the simulated values. There is, however, discrepancies in the values obtained as the convection cooling due to air is not effectively modelled in the simulation. IR thermographic images taken on the phone mimicking such a phone call is also shown in Fig. 9 at similar but not identical time intervals. It is important to note that measurement conditions are not identical in the

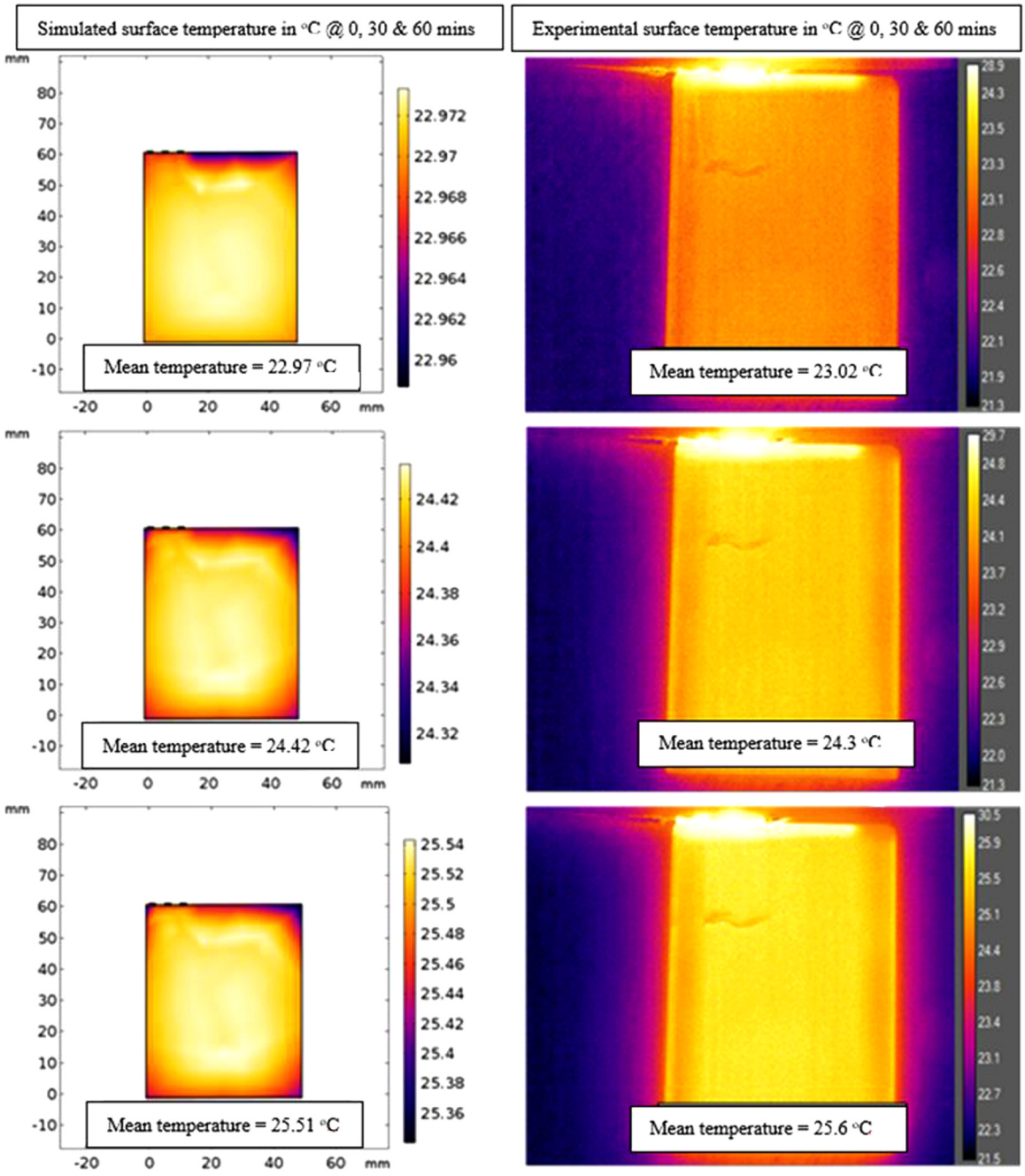

Fig. 6. A comparison of final temperature at the centre of the battery measured from simulated and experimental thermographic images taken for 0 (top) 30 Ω (middle) and 60 min (bottom) of use.

thermography experiment to those used in the simulation and the temperature sensor measurements. For example, to allow experimental IR thermography mimicking a phone call, we had use the whole assembly of the phone, for which the thermal load is slightly different than that for the battery only. Also, the phone had to be kept in air and not insulated inside a Styrofoam box to allow direct imaging. As such, thermographic images show a lower (~2 °C) initial temperature of the phone and its temperature values were ~3 °C lower than the simulated values and the sensor readings during the call at similar time intervals.

Overall, the model shows that the temperature was dominated by the CPU heat, conduction from which exceeded the contributions to the heating from the antenna and the battery. The antenna heat, however, has more penetrative properties and must not be ignored as the penetration means that temperature changes can travel deeper within the phantom, and cause temperature effects inside soft tissues.

3.5. Complete head model with simulation of mobile phone heating

Simulating the complete model involves the phone and its antenna. Combining the three sections with ambient cooling to the environment, the overall phone interaction can be estimated. A head model was also simulated in this set up. Combining the battery, circuit board, antenna and head model, a full depiction of the thermal effects of a mobile phone can be simulated. The key parameters for this simulation is a discharge of 0.6 A, mother board temperature of 35 °C and antenna power of 2 W at 1800 MHz. The phone was placed 25 mm from the head model (Fig. 10). The models arterial blood temperature was set to 310 °C. The time scale for this was 10 min.

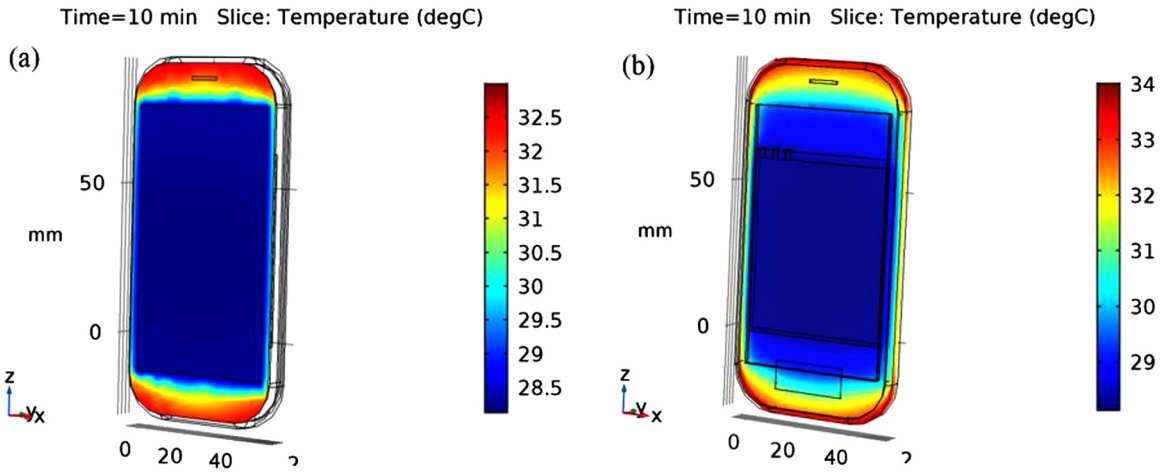

Fig. 7. Surface temperature of phone, screen temperature noted to be 27 °C, which agrees with surface temperature experiments. This value though, is heavily influenced by the surface materials thermal conductivity, plastic materials (used here) with a low thermal conductivity, whereas an aluminium body would have a high thermal conductivity and hence a higher surface temperature (a). Slice Temperature of phone shows that the battery temperature would be 27 °C and the circuit board ranges from 31 °C to 35 °C, both of which show agreeance to the experimental values measured. (b).

We compared the simulated data with thermographic images taken by Bauer et al. (2018) that examined heating effects of smartphones on the human auricle region. Fig. 12 shows a graphical comparison while Fig. 13 show a comparison of quantitative values. Temperature hotspots can be noticed in Fig. 12 (Left) especially around the ear, cheek and eye socket.

The importance of distance of the phone from the head model becomes evident from these models because convection heating dominates from the non-radiative heat as long as the phone is kept apart from the head model. If a contact is made with the phone to the surface of the head the heat transfer trough the conduction dominates, however.

The full phone model was then applied to the cube phantom. With this simpler phantom, it is easier to make variations parameters e.g. the phone distance. By varying this distance, the effects of conduction heating and convection heating can be compared for the phone model. From this simulation the difference in distance of the phone to the head can be investigated, 50 mm vs 0 mm (Fig. 11). An increase of temperature is 10 fold, 0.4 °C for the 50 mm away and 4 °C 0 mm away. In both instances, the antenna radiofrequency heating dominates the heating phenomena.

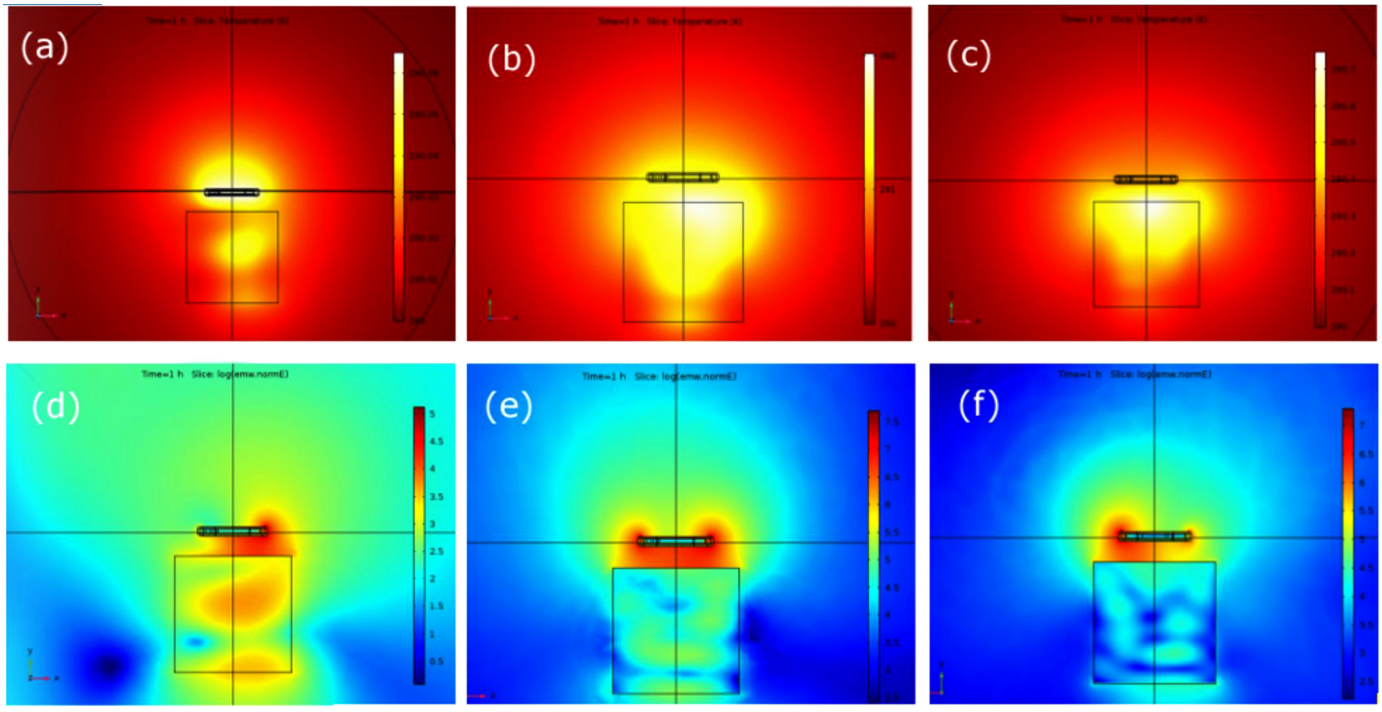

Fig. 8. a-c. Antenna heating effect simulated in a cube of skin/fat phantom showing the depth and areas of intensity of temperature, depth of heat penetration and the ability of the phantom to heat more than the air: @900 MHz maximum antenna temperature increase is nominal, ~0.06 °C (a); @1800 MHz antenna shows a much greater tendency to heat the phantom, with a maximum temperature reaching 19°C (b); @2250 MHz antenna temperature is similar to 900 MHz with a nominal change in temperature (c). d-f. Antenna electrical field effect simulated in a cube of skin/fat phantom showing the depth and areas of intensity of the logarithm of the electric field: high electromagnetic intensities in the cube and in the air between the cube and phone @900 MHz (a), intensity is distributed in the air around the phone and throughout the phantom cube @1800 MHz (b) and @2250 MHz (c).

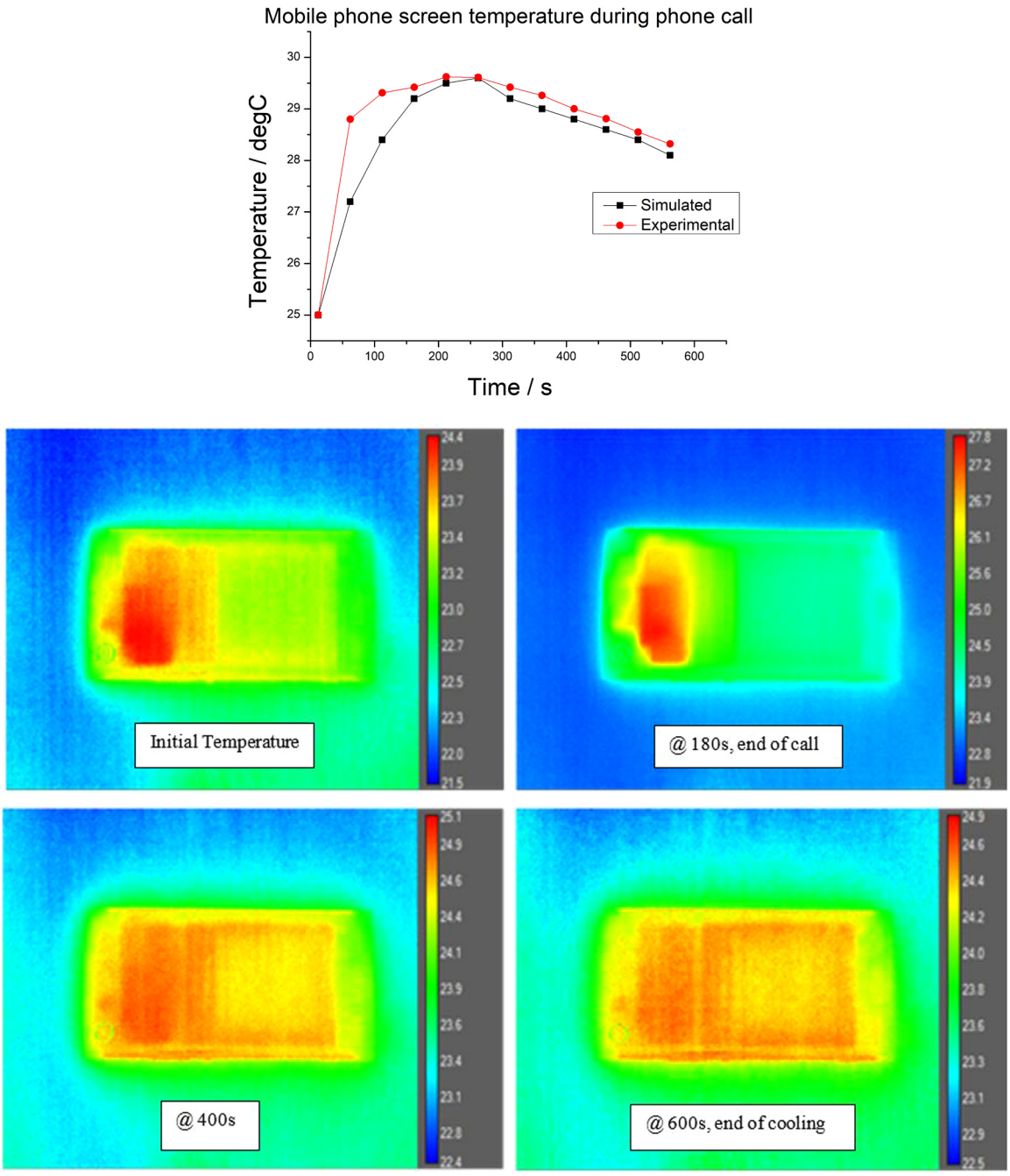

Fig. 9. A comparison of the mobile phone screen temperature extracted from simulation and temperature sensor at different times during and after a 200 s phone call starting at 12 s and ended after 212 s (top). Experimental IR thermographic images of the surface temperature of the phone is also shown at comparable time intervals: in the beginning, at the end of the call, during cooling and at the end of the cooling (bottom).

3.6. Comparison of simulated data with clinical data

Looking at the mean temperatures of the auricle changes during the experiment phase for the whole population studied in the clinical investigation of Bauer et al. (2018) we take the case of a 5-min phone call after which phone was allowed to cool while keeping the phone against the side of the head for another 60 min. In the simulation, we follow the results of such a 5-min phone call so as to determine the heating effects and conduction for a quantitative comparison of temperature values measured by IR thermography. The simulation was set up to have ambient temperature and cooling similar to that as the clinical study. Fig. 13 show an excellent agreement of the simulated data with the clinical data with a slightly higher value predicted in the simulated values within the duration of the call.

Comparing graphical distribution of temperatures in simulated and clinical experiment (Fig. 12), we observe that temperatures in the cheek region show a somewhat similar temperature distribution although they differ in their respective false colour intensities. The temperature hotspots on the thermographic images are higher, by a noticeable ~3 °C. This discrepancy perhaps indicate that temperature distribution arising from blood flow is probably more dependent of the material composition rather than the topography of the material. In that case, the phantom material should consider some compositional variation of the fat e.g. by taking into consideration of the material mimicking skin as well as fat in cheeks. In ears, we may have to consider the blood circulation in cartilage. The general agreement between simulated and

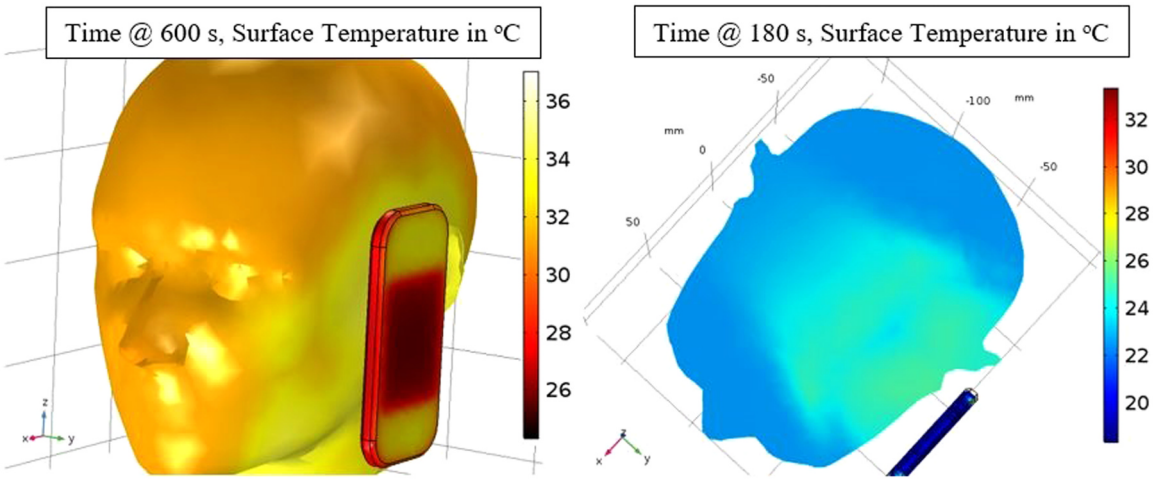

Fig. 10. Surface temperature of phone and head model, with noticeable heat increase to the face, on the side with the phone. 10 minutes of holding the phone next to the head model showed an increase from 30 °C to 33 °C (Left); x-y cross section temperature at 3 minutes, this shows a temperature increase from 25 °C to 27 °C (Right). The depth of the heating also for this phantom is ~100 mm into the head phantom.

clinical data in Figs. 12 and 13 is remarkable and highly encouraging to provide a solid foundation for future improvements towards applications in personalized and preventive medicine.

4. Conclusions

We have presented a detailed methodology and results of first principle modelling to simulate heating effect in human auricle region due to mobile phone use. In particular, our model considered both radiative and non-radiative heating from components such as the lithium ion battery, CPU circuitry and the antenna. We have successfully generated a model that can show the distribution and effect of the heating effect due to mobile phone use. Our simulated data has shown excellent agreement with clinical IR thermography images as well as quantitive, in vitro bench testing using temperature sensors and IR thermography. For the lithium ion battery model, comparable results to the validation experiment were achieved, the simulation proved to have an acceptable error from the validation, as the variation in each from the experimental value was less than 1%.

Our model can be used to determine the impact of various parameters on the discharge of phone batteries, along with the antenna parameters for the electromagnetic fields. The potential benefit of this model is for mobile phone design, the thermal and SAR aspects. Looking at the impacts of various battery parameters, the simulation has found that a) temperature increases with discharge rate, b) cathode materials show the highest temperature increase with LCO, the most commonly used commercial material, whereas LMO showed a temperature decrease c) temperature decreases with increase in battery capacity. The circuit board and battery combination proved effective, showing comparable results, the temperature across the phone, to an experimental test of phone temperatures. For the variation of antenna power and frequency, power directly increases RF heating.

For the frequencies active in mobile phones, 900 MHz, 1800 MHz and 2250 MHz, 1800 MHz showed the highest temperature increase in the fat/water phantom used in this simulation. 900 MHz and 2250 MHz showed similar heating, but below 1 °C. Varying the distance of the complete mobile phone model from the phantom cube, the temperature increased by a factor of 10 from contact with the phantom compared to 50 mm away. The model shows that the temperature was dominated by the CPU heat, conduction from and exceeded the contributions to the heating from the antenna and the battery. The antenna heat, however, has more penetrative properties. This allowed for temperature changes to travel deeper and cause much serious temperature effect on soft tissues and brain.

Potential improvements to the validation experimental would be better control with an ambient temperature being measured during the

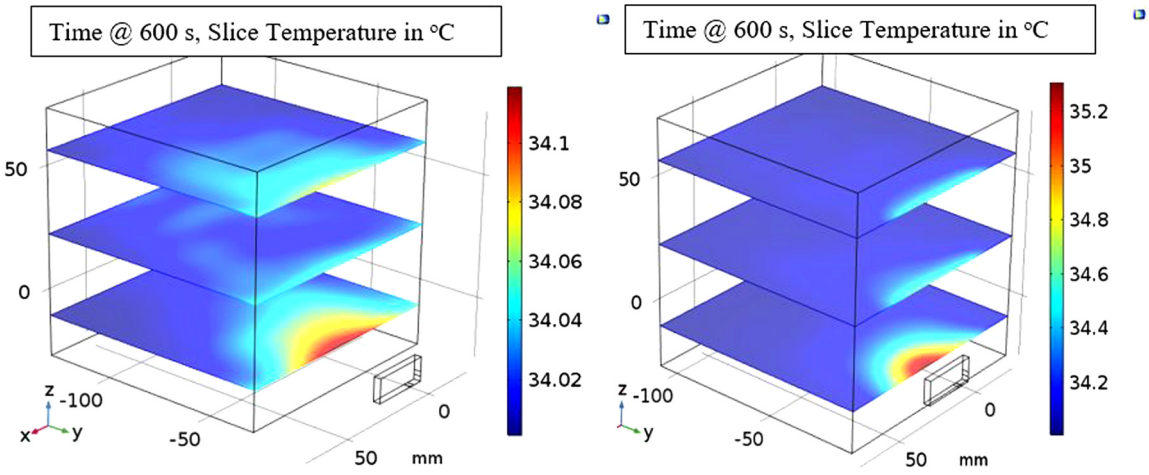

Fig. 11. Simulated temperature slices after 10 min of cube phantom, the main source of heating in the cube coming from the antenna, at a distance of 50 mm away from the cube (Left). Temperature slice after 10 min of cube phantom, with the phone being placed in contact with the cube, at a distance of 0 mm (Right).

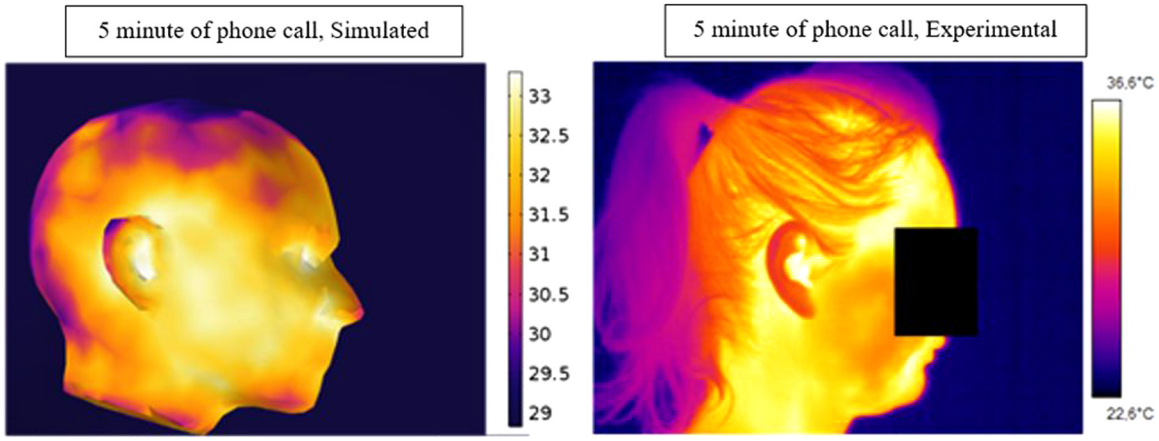

Fig. 12. Typical surface temperature distribution in human auricle region after 5 min of mobile phone call from simulation (Left) and clinical image (Right).

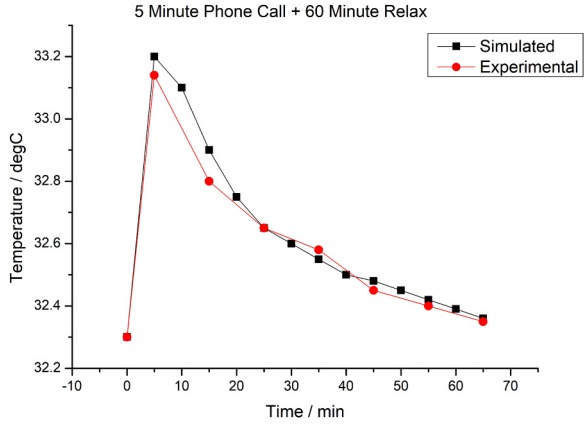

Fig. 13. A quantitative comparison of mean temperature of heating sections reported in clinical phone call experiment (Bauer et al., 2018) with that obtained from simulation in the present study.

logging, as well as having the ambient temperature the same across each discharge rate. Further developments in the predictive power of the model may include taking into consideration of the phantom materials' composition to mimic more realistically the composition of the tissue that is being modelled.

Acknowledgement

The authors acknowledges European Commission "Erasmus + Programme Inter-institutional Agreement 2017-2021" between Wroclaw University of Science and Technology, Poland and University of Limerick, Ireland for travel and training support. Ms. Sarah Markham is acknowledged for her support in experimental, *in vitro* infrared thermography of mobile phone heating.

Funding

This research did not receive any specific grant from funding agencies in the public, commercial, or not-for-profit sectors.

References

Abdel-Rassoul, G., El-Fateh, O.A., Salem, M.A., Michael, A., Farahat, F., El-Batanouny, E., Salem, E., 2007. Neurobehavioral effects among inhabitants around mobile phone base stations. Neurotoxicology 28 (2), 434–440.

Acharya, J.P., Acharya, I., Waghrey, D., 2013. A study on some psychological health effects of cell-phone usage amongst college going students. Int J. Med. Res Health Sci. 2 (3), 388–394.

Adair, E.R., Adams, B.W., Akel, G.M., 1984. Minimal changes in hypothalamic temperature accompany microwave-induced alteration of thermoregulatory behavior. Bioelectromagnetics 5, 13–30.

Agarwal, A., Deepinder, F., Sharma, R.K., Ranga, G., Li, J., 2008. Effect of cell phone usage on semen analysis in men attending infertility clinic: an observational study. Fertil. Steril. 89, 124–128.

Bauer, J., Gorecki, I., Kohyt, M., Migasiewicz, A., Podbielska, H., 2018. The influence of smartphones' operation modes on the superficial temperature distribution in the human auricle region: a small scale (n = 20) clinical examination. J. Therm. Anal. Calorim. 133 (1), 559–569.

Blackman, C.F., Benane, S.G., Kinney, L.S., Joines, W.T., House, D.E., 1982. Effects of ELF fields on calcium-ion efflux from brain tissue in vitro. Radiat. Res. 92, 510–520.

Blank, M., Goodman, R., 1999. Electromagnetic fields may act directly on DNA. J. Cell Biochem. 75, 369–374.

Borbely, A.A., Huber, R., Graf, T., Fuchs, B., Gallmann, E., Achermann, P., 1999. Pulsed high-frequency electromagnetic field affects human sleep and sleep electroencephalogram. Neurosci. Lett. 275, 207–210.

Cai, L., White, R.E., 2011. Mathematical modeling of a lithium ion battery with thermal effects in COMSOL Inc. Multiphysics (MP) software. J. Power Sources 196 (14), 5985–5989.

Chen, S.C., Wan, C.C., Wang, Y.Y., 2005. Thermal analysis of lithium-ion batteries. J. Power Sources 140 (1), 111–124.

Chen, X., Steckner, M., 2017. Electromagnetic computation and modeling in MRI. Med. Phys. 44 (3), 1186–1203.

Christ, A., Gosselin, M.C., Christopoulou, M., Kuhn, S., Kuster, N., 2010. Age-dependent tissue-specific exposure of cell phone users. Phys. Med. Biol. 55, 1767–1783.

Cleveland, R.F.S., David, M.U., Jerry, L., 1997. Evaluating compliance with fcc Guidelines for human exposure to radiofrequency electromagnetic fields. OST Bull. 65, 97–101.

Council of European Union, 1999. Council recommendation of 12 July 1999 on the limitation of exposure of the general public to electromagnetic fields (0 Hz to 300 GHz). Communities, pp. 59–70.

COMSOL Multiphysics® v. 5., ⟨www.comsol.com⟩. COMSOL AB, Stockholm, Sweden.

COMSOL Multiphysics®, 2011. C. Software, and L. Agreement. Absorbed Radiation (SAR) in the Human Brain. ⟨https://www.comsol.com/model/specific-absorption-rate-sar-in-the-human-brain-2190⟩.

De Iuliis, G.N., Newey, R.J., King, B.V., Aitken, R.J., 2009. Mobile phone radiation induces reactive oxygen species production and DNA damage in human spermatozoa in vitro. PLoS One 4 (7), e6446.

Deltour, I., Auvinen, A., Feychting, M., Johansen, C., Klaeboe, L., Sankila, R., Schüz, J., 2012. Mobile phone use and incidence of glioma in the Nordic countries 1979–2008: consistency check. Epidemiology 23 (2), 301–307.

Develi, I., Sorgucu, U., 2015. Prediction of temperature distribution in human BEL exposed to 900 MHz mobile phone radiation using ANFIS. Appl. Soft Comput. J. 37, 1029–1036.

Dreyer, N.A., Loughlin, J.E., Rothman, K., 1999. Cause-specific mortality in cellular telephone users. JAMA 282 (19), 1814–1816.

Durney C.H., Massoudi H., Iskander M.F., 1986. Radiofrequency Radiation Domismetry Handbook.

F.C. Commission, 2015. Consumer Guide, 1–3.

Goyal, A.K., 2015. Studies on phantom vibration and ringing syndrome among post-graduate students. Indian J. Comm. Health 27 (1), 35–40.

Ha, B.Y., 2001. Stabilization and destabilization of cell membranes by multivalent ions. Phys. Rev. E Stat. Nonlin. Soft Matter Phys. 64 (051902), 1–5.

Habash, R.W.Y., 2008. Bioeffects and Therapeutic Applications of Electromagnetic Energy. CRC Press, Boca Raton.

Hamada, A.J., Singh, A., Agarwal, A., 2011. Cell phones and their Impact on male fertility: Fact or fiction. Open Reprod. Sci. J. 5, 125–137.

Hepworth, S.J., Schoemaker, M.J., Muir, K.R., Swerdlow, A.J., Tongeren, M.J., McKinney, P.A., 2006. Mobile phone use and risk of glioma in adults: case-control study. BMJ 332 (883), 1–5.

Hosseinzadeh, E., Marco, J., Jennings, P., 2017. Electrochemical-thermal modelling and optimisation of lithium-ion battery design parameters using analysis of variance. Energies 10 (1278), 1–22.
Huber, R., Treyer, V., Borbely, A.A., Schuderer, J., Gottselig, J.M., Landolt, H.P., Werth, E., Berthold, T., Kuster, N., Buck, A., Achermann, P., 2002. Electromagnetic fields, such as those from mobile phones, alter regional cerebral blood flow and sleep and waking EEG. J. Sleep. Res. 11 (4), 289–295.
IARC, 2013. International Agency for Research on Cancer (IARC), IARC classifies radio-frequency electromagnetic fields as possibility carcinogenic to humans. (http://www.iarc.fr/en/media-centre/pr/2011/pdfs/pr208_E.pdf).
Iqbal-Faruque, M.R., Aisyah-Husni, N., Ikbal-Hossain, M., Tariqul-Islam, M., Misran, M., 2014. Effects of mobile phone radiation onto human head with variation of holding cheek and tilt positions. J. Appl. Res. Technol. 12 (5), 871–876.
Kargel, C., 2005. Infrared thermal imaging to measure local temperature rises caused by handheld mobile phones. IEEE Trans. Instrum. Meas. 54 (4), 1513–1519.
Kesari, K.K., Kumar, S., Behari, J., 2011. Effects of radiofrequency electromagnetic wave exposure from cellular phones on the reproductive pattern in male wistar rats. Appl. Biochem. Biotechnol. 164 (4), 546–559.
Khurana, V.G., Teo, C., Kundi, M., Hardell, L., Carlberg, M., 2009. Cell phones and brain tumors: a review including the long-term epidemiologic data. Surg. Neurol. 72, 205–215.
Kim, K.H., Kabir, E., Jahan, S.A., 2016. The use of cell phone and insight into its potential human health impacts. Environ. Monit. Assess. 188 (4), 221–238.
Koivisto, M., Krause, C.M., Revonsuo, A., Laine, M., Hamalainen, H., 2000a. The effects of electromagnetic field emitted by GSM phones on working memory. Neuroreport 22, 1641–1643.
Koivisto, M., Revonsuo, A., Krause, C.M., Haarala, C., Sillanmaki, L., Laine, M., Hamalainen, H., 2000b. Effects of 902 MHz electromagnetic field emitted by cellular telephones on response times in humans. Neuroreport 11, 413–415.
Komarov, V., Wang, S., Tang, J., 2005. Permittivity and measurements. Encycl. RF Microw. Eng. 3693–3711.
Krause, C.M., Haarala, C., Sillanmaki, L., Koivisto, M., Alanko, K., Revonsuo, A., Laine, M., Hamalainen, H., 2004. Effects of electromagnetic field emitted by cellular phones on the EEG during an auditory memory task: a double blind replication study. Bioelectromagnetics 25 (1), 33–40.
Krause, C.M., Sillanmaki, L., Koivisto, M., Haggqvist, A., Saarela, C., Revonsuo, A., Laine, M., Hamalainen, H., 2000. Effects of electromagnetic fields emitted by cellular phones on the electroencephalogram during a visual working memory task. Int. J. Radiat. Biol. 76 (12), 1659–1667.
Kundi, M., 2004. Mobile phone use and cancer. Occup. Environ. Med. 61 (6), 560–570.
Lahiri, B.B., Bagavathiappan, S., Soumya, C., Jayakumar, T., Philip, J., 2015. Infrared thermography based studies on mobile phone induced heating. Infrared Phys. Tech. 71, 242–251.
Lai, H., Singh, N.P., 1996. Single- and double-strand DNA breaks in rat brain cells after acute exposure to radiofrequency electromagnetic radiation. Int J. Radiat. Biol. 69, 513–521.
Lai, Y., Du, S., Ai, L., Cheng, Y., Tang, Y., Jia, M., 2015. Insight into heat generation of lithium ion batteries based on the electrochemical-thermal model at high discharge rates. Int. J. Hydrog. Energy 40 (38), 13039–13049.
Laurence, J.A., French, P.W., Lindner, R.A., McKenzie, D.R., 2000. Biological effects of electromagnetic fields-mechanisms for the effects of pulsed microwave radiation on protein conformation. J. Theor. Biol. 206, 291–298.
Li, S., Li, S., Anwar, S., Tian, F., Lu, W., Hou, B., 2014. Determination of microwave conductivity of electrolyte solutions from debye-drude model. In: Proceedings of the Progress in Electromagnetics Research Symposium 2, pp. 670–673.
Little, M.P., Rajaraman, P., Curtis, R.E., Devesa, S.S., Inskip, P.D., Check, D.P., Linet, M.S., 2012. Mobile phone use and glioma risk: comparison of epidemiological study results with incidence trends in the United States. BMJ 344, e1147 (1–16).
Mann, K., Röschke, J., 1996. Effects of pulsed high-frequency electromagnetic fields on human sleep. Neuropsychobiology 33, 41–47.
Mernyei F., Volgyi F., 1990. Simple methods for testing the temperature dependence of microstrip antenna arrays. In: Proceedings of the 20th European Microwave Conference 1, pp. 365–370.
Morgan, L.L., Kesari, S., Lee Davis, D., 2014. Why children absorb more microwave radiation than adults: the consequences. JMAU 2 (4), 197–204.
Neumann, E., Schaefer-Ridder, M., Wang, Y., Hofschneider, P.H., 1982. Gene transfer into mouse lyoma cells by electroporation in high electric fields. EMBO J. 1 (7), 841–845.
NTS News Center, 2016. X-Ray Computed Tomography (CT) Scanning & Battery Cells. ⟨https://www.nts.com/ntsblog/x-ray-computed-tomography-ct-scanning-battery-cells/⟩.
Oftedal, G., Wilen, J., Sandstrom, M., Mild, K.H., 2000. Symptoms experienced in connection with mobile phone use. Occup. Med. 50, 237–245.
Panagopoulos, D.J., 2011. Analyzing the health impacts of modern Telecomumications Microwaves. Adv. Med Biol. 17, 1–55.
Prasad, M., Kathuria, P., Nair, P., Kumar, A., Prasad, K., 2017. Mobile phone use and risk of brain tumours: a systematic review of association between study quality, source of funding, and research outcomes. Neurol. Sci. 38 (5), 797–810.
Robertson, V., Ward, A., Low, J., Reed, A., 2006. Electrotherapy Explained, Principles and Practice, 4th ed. Elsevier, Amsterdam.
Sanders, J.W., Yao, J., Huang, H., 2015. Microstrip patch antenna temperature sensor. IEEE Sens. 15 (9), 5312–5319.
Schüz, J., Jacobsen, R., Olsen, J.H., Boice, J.D., McLaughlin, J.K., Johansen, C., 2006. Cellular telephone use and cancer risk: update of a nationwide Danish cohort. J. Nat. Cancer Inst. 98, 1707–1713.
Simon, H.U., Haj-Yehia, A., Levi-Schaffer, F., 2000. Role of reactive oxygen species (ROS) in apoptosis induction. Apoptosis 5, 415–418.
Statista.com, 2016. Number of mobile phone users worldwide 2013–2019. ⟨https://www.statista.com/statistics/274774/forecast-of-mobile-phone-users-worldwide/⟩.
Statista.com, 2018. Frequency of making mobile phone calls by gender 2018 UK Survey. ⟨https://www.statista.com/statistics/466240/mobile-phone-use-by-frequency-of-calling-in-the-uk/⟩.
Tahvanainen, K., Niño, J., Halonen, P., Kuusela, T., Alanko, T., Laitinen, T., Länsimies, E., Hietanen, M., Lindholm, H., 2007. Effects of cellular phone use on ear canal temperature measured by NTC thermistors. Clin. Physiol. Funct. Imaging 27 (3), 162–172.
Tjaden, B., Cooper, S.J., Brett, D., Kramer, D.J., Shearing, P.R., 2016. On the origin and application of the Bruggeman correlation for analysing transport phenomena in electrochemical systems. Curr. Opin. Chem. Eng. 12, 44–51.
WHO.int, 2016. Electromagnetic fields and public health: mobile phones. ⟨http://www.who.int/news-room/fact-sheets/detail/electromagnetic-fields-and-public-health-mobile-phones⟩.

Joanna Bauer is an Assistant Professor in the Department of Biomedical Engineering at Wrocław University of Science and Technology, Poland. She received Ph.D. in Applied Physics, as well as a MSc. Eng. in Biomedical Engineering, and a MSc in Management and Marketing. Her main research activity focuses on infrared imaging. She is an author/co-author of more than 90 publications, 60 conference presentations, including over 20 plenary and invited lectures. Dr Bauer was a visiting scientist in a number of scientific institutions worldwide. She has been awarded several times for her professional achievements including e.g. Siemens Research Prize for Outstanding Achievements in Technology and Science.

Charlie O'Mahony is a Ph.D. researcher of the Department of Physics and Bernal Institute, University of Limerick, Ireland. He has a MSc in Advanced Engineering Materials and a BSc in Applied Physics from the same university. His research focusses on medical and industrial application of Infrared Imaging.

Drahomir Chovan is a Postdoctoral Research Fellow the Department of Physics and Bernal Institute, University of Limerick, Ireland. He has a Ph.D. in Physics from the same university and a Masters in Solid State Physics from the Comenius University of Bratislava, Slovakia. His specialises in first principle simulation of materials properties using quantum mechanical and phenomenological approaches.

John Mulcahy is one of the founding members of Modelling, Simulation and Innovative Characterisation (MOSAIC) group at the Bernal Institute. He has a MSc and BSc in Electrical and Computer Engineering from the University of Limerick. He has managed numerous European and industry projects developing materials, instruments, engineering and automation. His research interest includes cybernetics, security and translation of fundamental research into commercial products or technology.

Christophe Silien is a Lecturer in Nanoscience with the Department of Physics in the University of Limerick (Ireland) and is a member of the MOSAIC and Bernal Institute. He obtained his PhD in 2003 from the University of Namur, Belgium and worked as postdoctoral researcher in the University of California Irvine, USA and University of St Andrews, UK. He has established a research laboratory dedicated to the development and exploitation of linear/non-linear optical micro-spectroscopy and scanning probe methodologies that encompass research areas such as super-resolution, plasmonics, diagnostics, microfluidics for real time characterisation and non-destructive metrology.

Syed A. M. Tofail is an Associate Professor at the Department of Physics of University of Limerick,Ireland and a member of Bernal Institute of the same University. He received an M.Sc.and a B.Sc. in Engineering (Metallurgical) from Bangladesh University of Engineering and Technology (BUET), Dhaka, Bangladesh. After completing his Ph.D. in Physics at the University of Limerick, Ireland in 2002 he worked as a postdoctoral fellow and a Senior Research Fellow in the Materials and Surface Science Institute of the same university where he specialised on molecular modelling and surface characterisation using X-ray photoelectron spectroscopy. He used first-principle design of materials and interfaces for developing piezoelectric hydroxyapatite, radiopaque NiTi alloys, antimicrobial textiles, anti-encrustation stents and drug-eluting stents. He is one of the co-inventors of super-resolution chemical imaging using infrared absorption.